Tellus
SERIES A
DYNAMIC
METEOROLOGY
AND OCEANOGRAPHY
PUBLISHED BY THE INTERNATIONAL METEOROLOGICAL INSTITUTE IN STOCKHOLM

Tellus (2008), 60A, 848–862

TELLUS

Convergence of aqua-planet simulations with increasing resolution in the Community Atmospheric Model, Version 3

By DAVID L. WILLIAMSON*, *National Center for Atmospheric Research, Box 3000, Boulder, CO, USA*

(Manuscript received 19 September 2007; in final form 29 April 2008)

ABSTRACT

The convergence of simulations from the Community Atmosphere Model with increasing resolution is determined in an aqua-planet context. Convergence as a function of scale is considered. Horizontal resolution (T42–T340) and time step (40–5 min) are varied separately. The simulations are sensitive to both. Global averages do not necessarily converge with increasing resolution. The zonal average equatorial precipitation shows a strong sensitivity to time step. Parametrizations should be applied in a range of time steps where such sensitivity is not seen. The larger scales of the zonal average equatorial precipitation converge with increasing resolution. There is a mass shift from polar to equatorial regions with increasing resolution with no indication of convergence. The zonal average cloud fraction decreases with increasing resolution with no indication of convergence. Equatorial wave propagation characteristics converge with increasing resolution, however a relatively high truncation of T170 is required to capture wavenumbers less than 16. Extremes are studied in the form of the probability density functions of precipitation. The largest half of the scales of the model converge for resolutions above T85.

1. Introduction

For some time at least one journal in computational fluid dynamics (CFD) has required that acceptable papers reporting numerical solutions consider systematic truncation error testing and accuracy estimation (Roache et al., 1986). The policy was reaffirmed more recently (Freitas, 1993). While acknowledging that no standard method for evaluating numerical uncertainty is accepted by the CFD community, Freitas (1993) presented a list of guidelines which included, among others, the statement that solutions should be presented over a range of different grid resolutions to demonstrate grid-convergent results. Climate modelling groups have generally avoided explicitly addressing the question of convergence of simulations. Studies of the effect of increased resolution generally base their conclusions on comparisons of the simulated climate with the observed atmospheric climate, as opposed to explicitly addressing the issue of convergence. Recent studies of this nature include Stratton (1999), Roeckner et al. (2006) and Hack et al. (2006), which also provide references to much of the past work in this area. Climate model resolution studies traditionally start with a model that was intensively developed at a low or modest resolution with the goal of producing the closest fit attainable to observed climate statistics. This simulated climate is then compared to those produced by higher resolution versions which received only modest additional efforts at tuning adjustable constants in the parametrizations. Often in these studies, higher resolution has not resulted in a 'better' solution by the measure of climate fidelity, which is counterintuitive to the computational fluid dynamics community.

This raises the question: Do simulations from Atmospheric General Circulation Models (AGCMs) converge with increasing horizontal resolution? Pope and Stratton (2002) have considered this question of model convergence and changes in systematic errors. As the term systematic errors implies, they concentrated on convergence in terms of comparison with observed statistics. They provide an excellent summary of the past work in this area. Included in the more general question of convergence above is the question: Are the larger scales affected by the addition of smaller scales in the model, or does increasing the resolution simply add finer scales to the simulation? This issue is compounded by the fact that in the common atmospheric modelling approach to increasing resolution, finer scales are added to the forcing by including finer scales in the orography. However, even if the surface orography were held fixed, there is an almost discontinuous surface forcing introduced at the boundaries

* Correspondence.
e-mail: wmson@ucar.edu
DOI: 10.1111/j.1600-0870.2008.00339.x

between land, ocean and sea-ice which implies forcing of the small scales at or near the truncation limit. Such a continual introduction of smaller scales to the forcing might prevent convergence. A related question is: If the models converge, do they converge to the same large-scale statistical state with different dynamic cores or with different parametrization packages.

A more fundamental question is: Should simulations converge? After all, AGCMs are partitioned into two distinct components, a resolved fluid flow component which is approximated numerically and generally referred to as the dynamic core, and an unresolved component which is parametrized as functions of the resolved scales provided by the dynamic core. This parametrized component provides the forcing of the dynamic core which leads to a statistical climate equilibrium. One hopes that simulations should converge, at least for the large, resolved scales which are a forced fluid dynamics problem. Otherwise it is not a well posed modelling problem, or we do not formulate it in a well posed way.

Are there reasons to believe simulations if they do not converge? If models do not converge does it follow that they are incorrect? The term correct implying that they produce the right statistics for the situation being modelled by the right combination of processes. The common assumption would be 'yes' for the second question. It seems unlikely that one would luckily choose the one resolution that gives the correct answer while finer and coarser resolutions give incorrect answers. Of course the opposite is not necessarily true, that is, if a model converges it is not necessarily correct. However, one would have more confidence in the results if multiple schemes (both dynamic cores and parametrization suites) converged to the same statistical states.

How should convergence be defined? As mentioned above, the convergence sequence in atmospheric modelling always adds finer scales in the representation of the solution, and usually to the external forcing as well. In the atmosphere the amplitude of many fields decreases with decreasing scale, but they do so relatively smoothly. There is no spectral gap which would allow a clean separation of resolved and unresolved scales. Looked at from the other perspective should convergence be defined as a function of scale? In other words, do the the large-scales converge? Do coarser resolution models match the coarser scales of finer resolution models? Should we just examine the convergence of 'large' scales? In fact, should the smaller scales near the truncation limit at any resolution be believed? The linear response functions of finite difference operators applied in the dynamic component show that the smallest scales are in general not well approximated in both phase and amplitude. Spectral models are accurate at all scales in linear problems, but the non-linear interactions of the smallest scales are not properly represented. These are some of the questions considered in this paper. To do so we consider only a selection of climate statistics.

2. Experimental basis

The question of concern in this paper is the convergence with increasing resolution to a statistical climate equilibrium of the forced, dissipative system. There are indications that the basic numerical methods of the dynamic cores do converge for short term deterministic tests. In fact, scheme developers often study the convergence properties of their schemes when applied to standard tests such as those for the shallow water equations of Williamson et al. (1992). Recent examples of such studies include Layton and Spotz (2003), Giraldo et al. (2003), Giraldo and Rosmond (2004) and Nair et al. (2005). In general numerical schemes do converge with such tests, the tests being rather large-scale and deterministic. In fact, lack of convergence generally rules out a scheme from further consideration. There are also indications that dynamic cores applied to idealized unstable flows converge with increasing resolution to within an uncertainty which is unavoidable in an unstable system (Jablonowski and Williamson, 2006a, 2006b).

As mentioned above, a complication in considering the convergence of AGCMs with increasing resolution is that, in their traditional application, the forcing scales decrease with increased resolution, for example, orography and underlying surface types. To avoid this complication we consider a simpler scenario in which the scale of the external surface forcing is fixed—an aqua-planet. The aqua-planet is covered with water and has no mountains, land or sea-ice. The sea surface temperatures (SST) are specified, usually with rather simple geometries such as zonal symmetry as in our case. The aqua-planet approach includes the full complexity of the atmospheric model including the parametrization suite, but simplifies the lower boundary exchange by defining a less complex surface. A diurnal cycle in radiation is included with the sun remaining over the equator. Specified radiative gasses such as ozone are symmetrized about the equator as is the SST so the climate is expected to be symmetric about the equator. Our experiments are all based on the 'CONTROL' case of Neale and Hoskins (2000) which is also a scenario in the Aqua Planet Experiment (APE) (http://www.met.reading.ac.uk/~mike/APE/). The specified SST in $^\circ$C is given by $27[1 - \sin^2(3\varphi/2)]$ for latitude φ between $\pm\pi/3$ and 0 elsewhere. This field is well represented by the lowest spectral resolution we consider. The maximum difference between the field truncated to T42 and the analytic field is the order of 0.0005 K giving about 5 digits of agreement.

Since there is no land–sea contrast, no mountains and no longitudinal variation in the SST, there is no forced component of the solutions, and the climate consists primarily of free motions. The 'correct' solutions of aqua-planet tests are not known. Nevertheless, it does appear to be a simpler environment to examine the convergence issue, perhaps providing a necessary condition. If convergence is not found there is no reason to expect the free motions of the normal AGCM to converge, even if a forced component does.

3. Model description

The AGCM used here is the Community Atmosphere Model Version 3 (CAM3) developed as the atmospheric component of the Community Climate System Model (CCSM3) in which it is coupled to active ocean, land and sea-ice models (Collins et al., 2006a). An overview of the CAM3 is provided by Collins et al. (2006b) and a complete technical description by Collins et al. (2004). The default dynamic core, which is used here, is based on the Eulerian spectral transform method (Machenhauer, 1979). The truncations considered are T42, T85, T170 and T340 with transform grids of approximately 2.8°, 1.4°, 0.7° and 0.35°, respectively. We do not vary the vertical resolution since the CAM3 parametrization suite is known to be very sensitive to the vertical resolution. We use the 26-level vertical grid of the standard configuration. The ∇^4 diffusion coefficients are set at 1.0×10^{16}, 1.0×10^{15}, 1.5×10^{14} and 2.25×10^{13} m^4 s^{-1} for the T42, T85, T170 and T340 truncations, respectively. These are the standard values used in the CAM3 for the lower resolutions. The values for all resolutions were determined experimentally with the model configured for atmospheric simulations, as opposed to aqua-planet simulations, so that in the mid to upper troposphere the kinetic energy spectra have reasonably straight tails for each resolution. Boville (1991) describes the approach. The two-dimensional spectra are shown in Fig. 1. Except for a small upturn at the ends, the spectra all have a slope close to -3, and lie very close to each other. The damping time scales at each truncation limit are 14.0, 8.6, 3.6 and 1.5 h for the T42, T85, T170 and T340, respectively. Note that these damping timescales decrease with increasing resolution. We have also repeated T42 and T85 simulations with a more scale selective ∇^6 damping. It had negligible impact on the fields described in the following as will be mentioned in passing in the relevant discussions.

The simulations start from a state taken from a previous aqua-planet simulation, possibly interpolated from a different resolution, and are run for 14 months. The analyses are over the last 12 months. When starting from a closely related aqua-planet state, the model transitions to its own aqua-planet climate in less than 2 months. We have run a few lower resolution aqua-planet experiments longer and established that 12 month samples are adequate for the statistics considered here, although we do not perform statistical significance testing in this paper. The highest resolution simulations were too expensive to run longer to allow that. Of course, the use of 12 month samples excludes the consideration of low frequency variability.

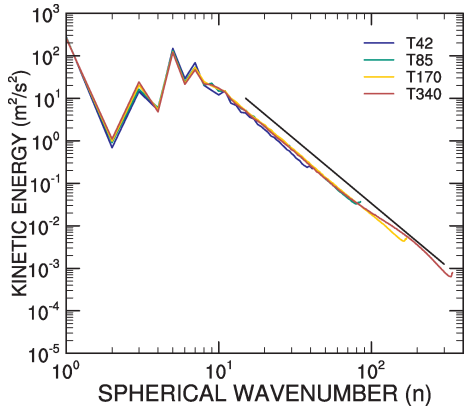

Fig. 1. Kinetic energy spectra AT 250 mb as a function of two-dimensional wavenumber for the T42, T85, T170 and T340 aqua-planet simulations. The straight line has a k^{-3} slope.

4. Example of resolution sensitivity

As mentioned above, studies of the effect of increased resolution in climate models are traditionally based on comparisons of the simulated climates of tuned models at different resolutions with the observed climate. We first consider such a comparison of tuned models, but without inclusion of observed values since the climate of the aqua-planet is not known. The models were tuned with regard to atmospheric simulations as described in the introduction, but applied here to the aqua-planet scenario. Figure 2a shows the time averaged, zonal averaged total precipitation produced by the default T42 and T85 released versions of CAM3. The precipitation is highly sensitive to 'resolution', with the peak tropical T85 values being nearly 50% larger than the T42 values. Both resolutions show double maxima separated by a minimum over two grid points, one on each side of the equator. The exact cause of the equatorial minimum precipitation occurring over the maximum in SST remains a modelling mystery. Williamson and Olson (2003) studied its dependence on time step and offered an explanation for that dependency while Williamson (2008) indicates a sensitivity to dynamic core. However the exact cause of the formation of a double versus single equatorial structure is not understood. Very little sensitivity is seen in the precipitation in mid to high latitudes. The 'resolution' change in this comparison actually consists of a number of changes which are easily isolated in a spectral transform model. One possible sequence of these changes, going from lower to higher resolution is: (1) reduction of time step required to maintain computational stability at the higher resolution, (2) reduction in grid interval, (3) increase in spectral truncation wavenumber consistent with the reduction in grid interval, (4) decrease in horizontal diffusion often scaled to keep the damping of the smallest resolved waves the same and (5) change in adjustable constants associated with different tuning of the parametrization suite for the two resolutions. The running accumulation of this sequence of changes is shown in Figs. 2b–f. Figure 2b shows the effect of the decreasing the time step from the T42 value (40 min) to the T85 (20 min), but maintaining all other aspects as in the standard T42 model. The time steps listed here are those over which the parametrizations are applied and correspond to the centred $2\Delta t$ of the Eulerian spectral transform dynamic core. The minimum in precipitation at the equator

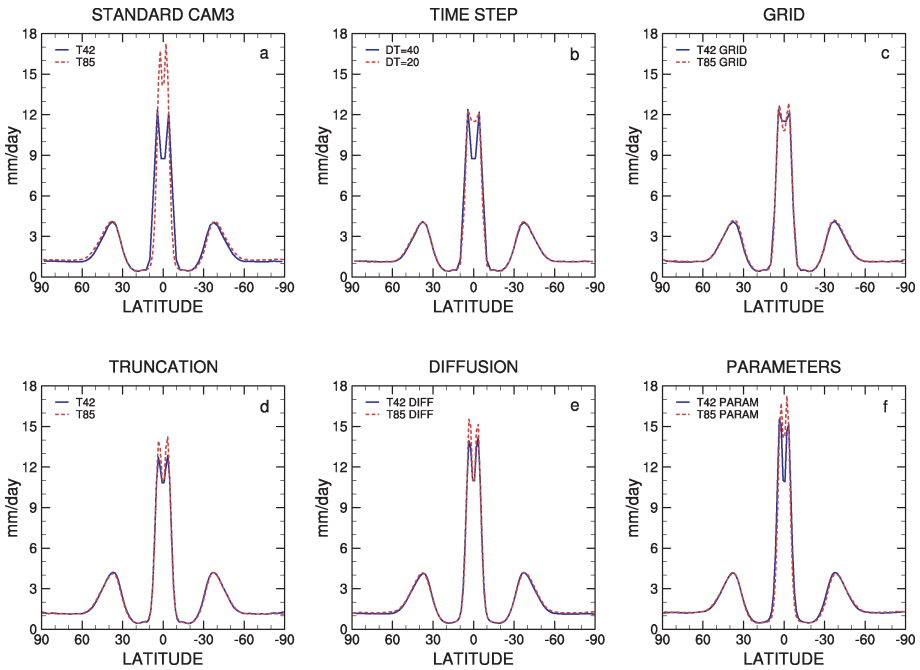

Fig. 2. Time averaged, zonal averaged precipitation from (a) default T42 and T85 CAM3, (b) T42 with $\Delta t = 40$ and 20 min, (c) T42, $\Delta t = 20$ min on T42 and T85 grids, (d) $\Delta t = 20$ min, T85 grid with T42 and T85 truncation, (e) $\Delta t = 20$ min, T85 grid, T85 truncation with T42 and T85 diffusion and (f) $\Delta t = 20$ min, T85 grid, T85 truncation and diffusion with T42 and T85 tuned adjustable constants.

in the standard T42 simulation is largely eliminated, while the peaks just off the equator are hardly changed. Williamson and Olson (2003) discuss the dependence of precipitation on the time step in the Community Climate Model (CCM3), a predecessor of CAM3. The behaviour here in CAM3 is similar. Figure 2c shows the effect of decreasing the grid interval from the T42 quadratic grid to the T85 grid while maintaining the T42 truncation and T85 time step. There is an increase in the maximum precipitation off the equator and decrease in the equatorial minimum. Figure 2d shows the effect of increasing the truncation to T85, maintaining the T85 time step and grid. The maximum off-equator values increase further. Figure 2e shows the effect of decreasing the diffusion coefficient from the standard T42 value to the standard T85 value, maintaining the T85 time step, grid and truncation. The maximum off-equator values increase even further. Finally, Fig. 2f shows the effect of changing the adjustable constants in the parametrization suite from those of the tuned T42 model to those of the tuned T85. Here the overall equatorial precipitation increases. Figure 2 shows that each aspect of the 'resolution' change has a rather modest effect, but accumulated they give the large change seen in Fig. 2a.

In this paper, we consider the convergence of the dynamic core with increasing resolution. Therefore, in the following we do not change the adjustable constants in the parametrization suite since such changes might confuse any basic dynamic core convergence signal. All subsequent experiments use the standard T85 values of the adjustable constants in the parametrization suite. Unlike with the spectral transform formulation, in many numerical approximations it is not obvious how to separate the grid resolution, effective truncation and diffusion from each other. For example, in grid-point based approximations, the truncation is often locked to the grid interval, and the numerical approximations often include an inherent diffusive component. Therefore, we combine these effects here, that is, grid, truncation and diffusion, and refer to that combination as resolution. We consider the time step size separately.

5. Global averages

We first consider the convergence of global averages of a few variables as the time step decreases and the resolution increases. Table 1 lists the time averaged, global averaged precipitable water for T42, T85, T170 and T340 truncations and 40, 20, 10 and 5 min time steps. The spectral transform model uses centred time differencing and the parametrizations are calculated over

Table 1. Time average, global average precipitable water (mm)

Δt	40	20	10	5
T42	19.57	19.88	20.03	20.21
T85		19.39	19.54	19.63
T170			19.18	19.13
T340				18.75

a $2\Delta t$ centred interval. We refer to that centred interval here as the time step We note that the corresponding time steps for the spectral model are traditionally listed as $\Delta t = 20$, 10, 5 and 2.5 min for T42, T85, T170 and T340 truncations, respectively. We prefer to use the parametrization interval since the time step sensitivity to be examined next is due to the parametrizations, not the dynamic core, and it will make for clearer comparisons with two-time-level schemes elsewhere (Williamson, 2008). In the tables and following figures not all time steps are included for all horizontal resolutions; the longer ones are excluded with the higher resolutions where the dynamic core is computationally unstable. The CAM spectral transform model requires that the parametrizations use the same centred time step as the dynamic core.

Table 1 shows that at the lower resolutions, T42 and T85, the global average precipitable water increases with decreasing time step. The increase is slightly less for T85 than for T42 over the same time step range. The increase is relatively small, being around 1% for the T85 model. The T170 shows a slight decrease in precipitable water for time step decreasing from 10 to 5 min. There is a much stronger variation with resolution. With the 5 min time step, the precipitable water decreases by around 7.5% from T42 to T340. The change for a doubling of resolution decreases with increasing resolution. With regard to an overall signal, the change in precipitable water with time step is in the opposite sense as the change with resolution. That is, normally the time step decreases as the resolution is increased to maintain computational stability, following the diagonal in the Table rather than a row or column. In that case the two effects partially cancel. However for precipitable water the time step signal is weaker and the resolution signal dominates.

The time averaged, global averaged total precipitation and its convective and stable components are summarized in Table 2. The total precipitation increases slightly with decreasing time step at the lower resolutions but shows no change at T170. The precipitation increases with increasing resolution. Here the change with time step is in the same sense as the change with resolution, and the two would combine in a traditional resolution change. The resolution signal is greater than the time step signal. Although not shown in the table, the global average clouds decrease at all levels with increasing resolution. Thus the long- and short-wave cloud forcing both decrease in magnitude and the net surface long wave and solar fluxes increase in magnitude. The solar increases more than the long wave leading to the increase in latent heat flux and a very slight increase in sensible heat flux. The clear sky fluxes show little variation with resolution so the change in precipitable water is not playing a role. Table 2 shows that the convective precipitation decreases with increasing time step and with increasing resolution while the stable increases with both changes. Again the changes are greater with resolution than with time step, and the change with time step is in the same sense as the change with resolution. Thus the two effects combine to yield a stronger signal.

Table 2. Time average, global average precipitation (mm d^{-1})

Δt	40	20	10	5
Total precipitation				
T42	2.74	2.78	2.79	2.82
T85		2.94	2.96	2.97
T170			3.06	3.06
T340				3.11
Convective precipitation				
T42	1.85	1.80	1.74	1.71
T85		1.76	1.66	1.59
T170			1.55	1.44
T340				1.36
Stable precipitation				
T42	0.89	0.98	1.05	1.11
T85		1.17	1.30	1.38
T170			1.51	1.62
T340				1.75

There is no indication that either precipitable water or precipitation has converged by T340. For fixed time step, the differences between adjacent resolutions are decreasing approaching the highest resolution but they have not reached zero. Note also that the convective precipitation decreases and the stable increases with increasing resolution. The stable variation is stronger than the convective leading to the increase in the total with decreasing time step and increasing resolution. Generally, people accept this change in the partition between convective and stable, arguing that more of the precipitation is explicitly resolved with increased resolution and therefore treated as stable. However, perhaps this collective wisdom should be challenged. Convective precipitation is usually thought to occur on scales even smaller than T340 and these are not resolved in any of these simulations. In addition, the stable precipitation is parametrized as a different mechanism.

6. Zonal averages

We continue to analyse precipitation by now considering the zonal average in the tropics which is shown in Figs. 3a–c for resolutions T42, T85 and T170 as a function of time step. The T42 simulations (Fig. 3a) show an increase in the equatorial precipitation with decreasing time step, with the maxima almost doubling from the longest to the shortest time step. Most of the change occurs from 40 to 10 min, with only a small additional change from 10 to 5 min. The shape changes from a tendency to form a double maxima with the longest time step to single maxima at shorter time steps. This property has been discussed by Williamson and Olson (2003). The T85 simulations (Fig. 3b) also show a large increase going from 20 to 10 min, again with a smaller increase from 10 to 5 min. It also shows the shape change from the longest to the shorter time steps. The T170

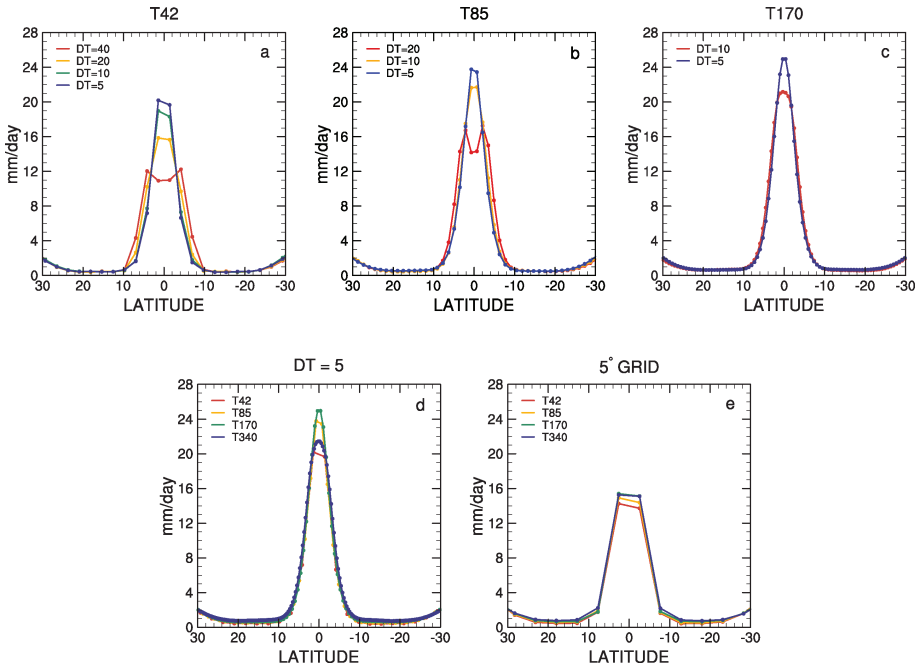

Fig. 3. Time averaged, zonal averaged precipitation from (a) T42 with $\Delta t = 40$, 20, 10 and 5 min; (b) T85 with $\Delta t = 20$, 10 and 5 min; (c) T170 with $\Delta t = 10$ and 5 min; (d) T42, T85, T170 and T340 with $\Delta t = 5$ min and (e) T42, T85, T170 and T340 with $\Delta t = 5$ min averaged to 5° grid.

simulation (Fig. 3c) shows a relatively small change going from 10 to 5 min. With the shortest time steps, the simulations do appear to be converging at each resolution in that the differences are getting smaller, but convergence has not been reached at the 5 min time step.

Figure 3d shows the tropical precipitation as a function of horizontal resolution with the 5 min time step. The variation with resolution is smaller than the variation with time step. The maxima increase from T42 to T85 to T170, then decrease to T340. The actual peak becomes narrower with increasing resolution so some of this variation may be due to the smaller scales which are included in the higher resolution representations. Figure 3e shows the precipitation when the values in Fig. 3d are conservatively averaged to a common 5° grid. Here there is a slight variation from T42 to T170 with the T170 and T340 values matching. Perhaps the larger scales in the tropics have converged when the time step sensitivity is excluded. One can just make out a variation with resolution in the minima on the flanks of the maxima. This, along with variation in the mid latitudes is responsible for the variation in the global averages seen earlier.

We now consider the convergence of the large-scale component of the zonal average for two other fields, excluding the time step sensitivity. Figure 4 shows the time averaged, zonal averaged surface pressure for T42, T85, T70 and T340 for the total field, and for a few selected latitudinal modes, all with the 5 min time step. Since the forcing and resulting zonal averages are symmetric about the equator, the two hemispheres are averaged to reduce the sampling variability slightly. The figures therefore just show the pole to equator domain. Since the zonal average is taken the modes are symmetric associated Legendre functions (P_n^m) with zonal wavenumber $m = 0$. The total field is shown top, left-hand panel. This panel indicates a shift in the atmospheric mass from polar to equatorial regions with increasing resolution. The mean, $n = 0$, is not shown. The model conserves the dry mass of the atmosphere by design so any variation in the mean of surface pressure is due to the variation in precipitable water discussed above in Section 5. That variation is small enough to not be distinguishable when plotted with the ordinate range used in the graphs of Fig. 4. The first symmetric component ($n = 2$) is shown top, centre. A portion of the mass shift is in this largest scale. The remainder is in the next mode ($n = 4$) shown top, right-hand side. The antisymmetric modes average to zero for the hemispheric presentation. However, their amplitudes are negligible when the hemispheres are considered separately, as expected. The next higher mode ($n = 6$) is shown bottom left-hand side. Here there is only a small variation with resolution. Note that all panels in Fig. 4 have the same ordinate range of 40 mb. The next pair of modes, $n = 8$ and 10 (bottom centre panel), also have only a small variation with resolution, while the remaining modes, $n = 12$ through the truncation limit (bottom, right-hand panel) show no variation. Thus the mass shift is represented by the two largest symmetric modes, $n = 2$ and 4, and these largest scales show no sign of convergence. There is a possibly that the mass shift is due to a very small but systematic tendency introduced by the mass fixer that is included in the model (Collins et al., 2004). An experiment with the mass fixer

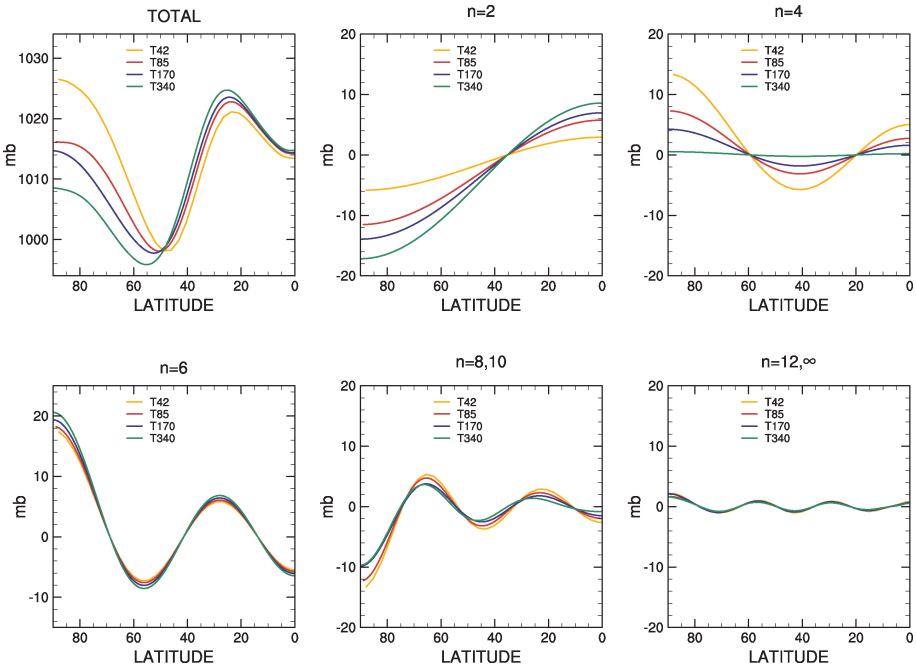

Fig. 4. Time averaged, zonal averaged surface pressure for T42, T85, T170 and T340 with $\Delta t = 5$ min, total and for specified symmetric spherical harmonics (P_n^m), $m = 0$: $n = 2$; $n = 4$; $n = 6$; $n = 8$ and 10; and $n = 12$ through the truncation limits.

turned off (not shown) indicates that this is not the case. The mass shift is associated with increasing poleward transport of angular momentum with resolution, driving both stronger mid-latitude westerly winds and easterly trade winds (not shown). The jet core itself, which forms around 30° latitude, becomes weaker with increasing resolution.

Figure 5 shows the time averaged, zonal averaged cloud fraction for T42, T85, T70 and T340 all with 5 min time step for

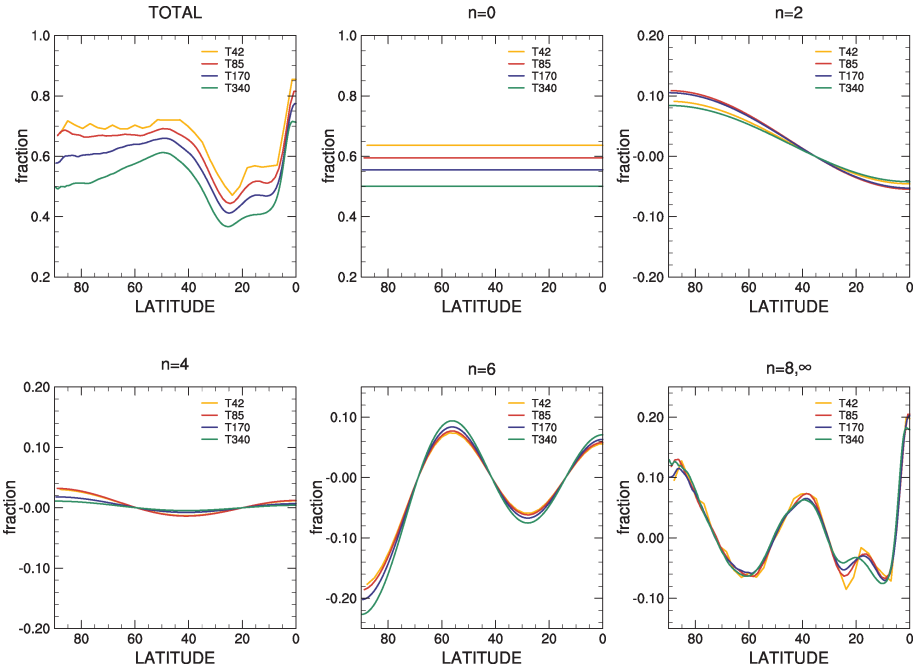

Fig. 5. Time averaged, zonal averaged cloud fraction for T42, T85, T170 and T340 with $\Delta t = 5$ min, total and for specified symmetric spherical harmonics (P_n^m), $m = 0$: $n = 0$; $n = 2$; $n = 4$; $n = 6$ and $n = 8$ through the truncation limits.

selected latitudinal modes. We note that surface pressure (p_s) discussed above is spatially smoothly varying and analysis of spectrally truncated components is natural, even though (ln p_s) rather than p_s is the spectrally represented prognostic variable. Instantaneous cloud fraction values are discontinuous and therefore not amenable to spectral truncation. However the time average, zonal average field is reasonably smoothly varying and examination of spectrally truncated states is reasonable and informative. Figure 5 upper left-hand side shows the total zonal average. A strong resolution signal is seen which is primarily in the global average ($n = 0$), shown top centre. The decrease with resolution appears to be the largest between the two highest resolutions which is opposite what one would see if the fields were converging with increasing resolution. The first ($n = 2$), second ($n = 4$) and third ($n = 6$) symmetric modes show a relatively small variation with resolution. Again, the antisymmetric modes are zero in the hemispheric average, but their amplitudes are actually negligible. Note that the range of the ordinate for the untruncated and $n = 0$ graphs (0.8) is twice that of the other panels, which are all the same (0.4). In the polar region these modes tend to have the same signal with resolution, adding minimally to the variation there, although the variations for some of the bands are not monotonic over the full range of resolutions. The remaining modes, lower right-hand side, ($n = 8$ through the truncation limit) show some variation in the smaller scales at the equator and on the flanks of the ascending branch of the Hadley cell.

7. Equatorial wave propagation

We now consider the equatorial wave propagation characteristics of the simulations via wavenumber-frequency diagrams following the spectral analysis methodology of Wheeler and Kiladis (1999). Figure 6 shows the log of the power of the symmetric component of the unnormalized spectra of the precipitation averaged from 10°S to 10°N. We plot the full power without removing a background spectrum in order to allow a comparison of the overall power of the waves. Normalization by a smooth background field such as done by Wheeler and Kiladis isolates spectral peaks that are often associated with specific normal modes or waves, but since the normalization is done individually for each model, the overall resolution signal associated with the power is contained in the background spectrum. Figure 6 includes the conventional dispersion curves (unlabeled) for odd meridional mode-numbered equatorial waves for equivalent depths of 12, 25 and 50 m (see Wheeler and Kiladis, 1999). The curves in the upper half of the plots show westward and eastward propagating inertio-gravity waves. The diagonal lines from bottom centre to the right-hand side are the eastward propagating Kelvin modes and the lower curves to the left-hand side are the westward propagating equatorial Rossby waves. The period decreases with increasing equivalent depth in each set.

The left-hand column of Fig. 6, top to bottom, shows the power from the T42 simulations with 40, 20, 10 and 5 min parametrization time steps. The right-hand column shows the power from the T85 simulations with 20, 10 and 5 min time steps. The T42, 40 min time step simulation (top left-hand side) shows a belt of increased power above the 50m equivalent depth Kelvin mode line. In general the power in this belt decreases with decreasing time step. There is an isolated eastward propagating wavenumber six peak with period between 6 and 10 d. This is independent of time step. Overall, the power in the lower frequencies tends to increase with decreasing time step. There is a very low frequency eastward propagating wavenumber five component with period longer than 30 d. The amplitude of this feature varies greatly in very long runs. Thus the 1-yr samples used here are too short to allow comparison of the amplitude of this feature. This low frequency, wavenumber five variability is discussed by Watanabe (2005, 2007) and Cash et al. (2007). The T85 simulations also show a general increase of the power in the lower frequencies with decreasing time step. The isolated wavenumber six peak with period between 6 and 10 d is visible with the 20 min parametrization time step but gets swamped by the overall increase of power with decreasing time step.

The left-hand column, top to bottom, of Fig. 7 shows the power as a function of resolution from T42 to T340 for the experiments with the 5 min parametrization time step. The power of both eastward and westward propagating waves increases with increasing resolution, most noticeably from T42 to T85, but from T85 to T170 as well. The power of the T340 looks quite similar to that of T170, perhaps indicating convergence, at least to within the noise attributable to the relatively short samples in the analyses. There is a significant increase in power going from T42 to T85 at all periods and wavenumbers. The belt of increased power associated with Kelvin modes seen in T42 is not as notable in T85, nor is the isolated wavenumber six feature. Comparing T170 power with that of T85 shows an increase in power along the 25 m equivalent depth Kelvin mode line.

The T85 and higher resolutions also show a block of power covering wavenumber 0 and eastward propagating wavenumbers 1 and 2 with period between 15 and 30 d which is missing from the T42. Power in this region of the plot, but with periods longer than 30 d, is associated with the MJO. However higher wavenumbers usually show power as well. These higher wavenumbers in the atmospheric analysis may be a result of geographical forcing and restriction associated with land–sea contrasts not present on the aqua planet. Atmospheric simulations with CAM3 develop a weak MJO with shorter than observed period.

The right-hand column, top to bottom, of Fig. 7 shows the ratios of the log of powers of the T42, T85 and T170 to the log of power of the T340. Note that the log of the power of the total field is negative because of the units of the original field. Thus higher power actually has a smaller magnitude. Thus for Fig. 7 the

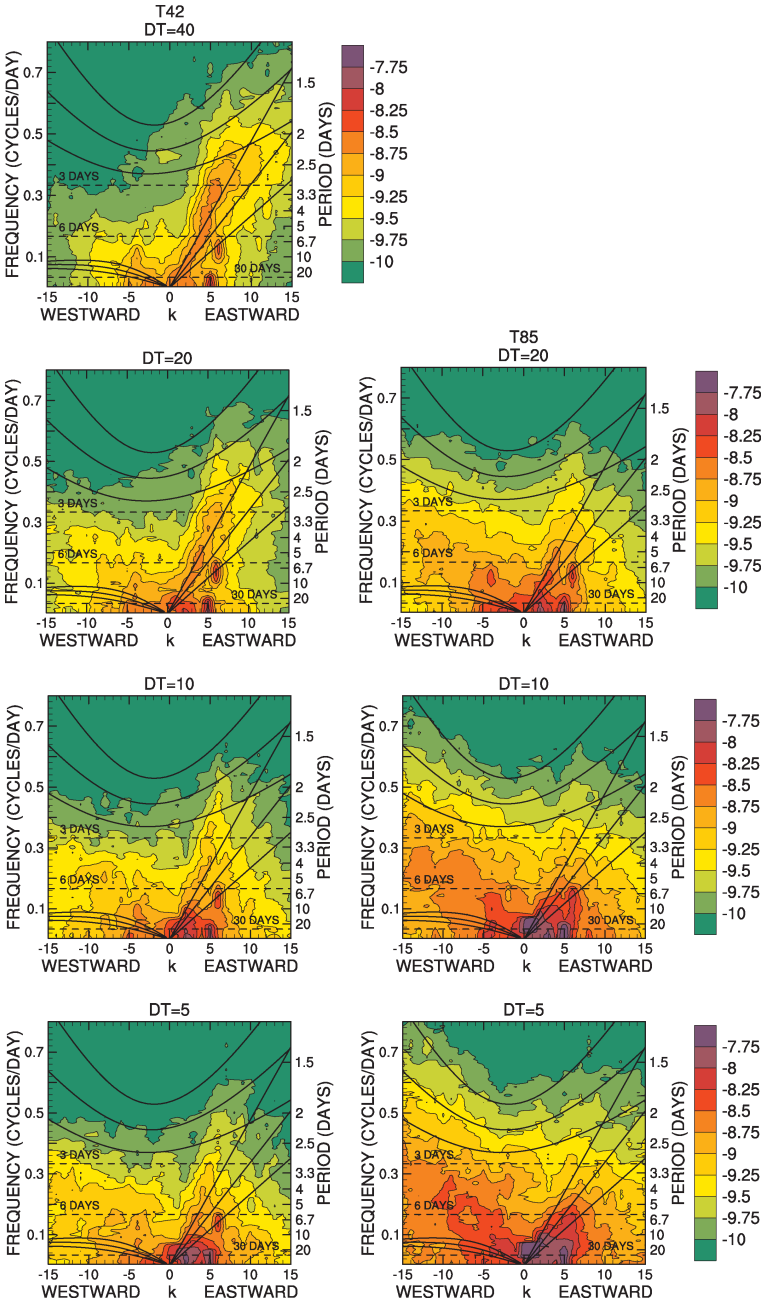

Fig. 6. Wavenumber-frequency diagrams of log of power of equatorial precipitation for (left-hand column) T42 with $\Delta t = 40$, 20, 10 and 5 min; and (right-hand column) T85 with $\Delta t = 20$, 10 and 5 min.

log-power of the T340 is divided by that of the lower resolution so that values of the ratio that are less than one imply less power in the lower resolution and values greater than one imply more power in the lower resolution. Overall, the ratio is near one with the T170, implying convergence. Thus a relatively high resolution of T170 is required to capture the propagating waves with wavenumbers less than 16. As mentioned earlier, we also performed T42 and T85 calculations with ∇^6 diffusion instead of the standard ∇^4. Plots from these runs show no significant differences with the corresponding ones of the standard model in Fig. 7.

8. Probability density function of precipitation

The probability density function provides information about the extremes simulated by the model. In this section we consider the probability density function of 6-h averaged precipitation in the equatorial region calculated from all grid points between 10°S and 10°N. Figure 8 shows pairs of plots; the left ones giving the fraction of the time the precipitation is in each 1 mm d^{-1} bin ranging from 0 to 120 mm d^{-1}, the right ones giving the fraction of the time the precipitation is in each 10 mm d^{-1} bin ranging from 0 to 1200 mm d^{-1}. In each plot the left-most bin

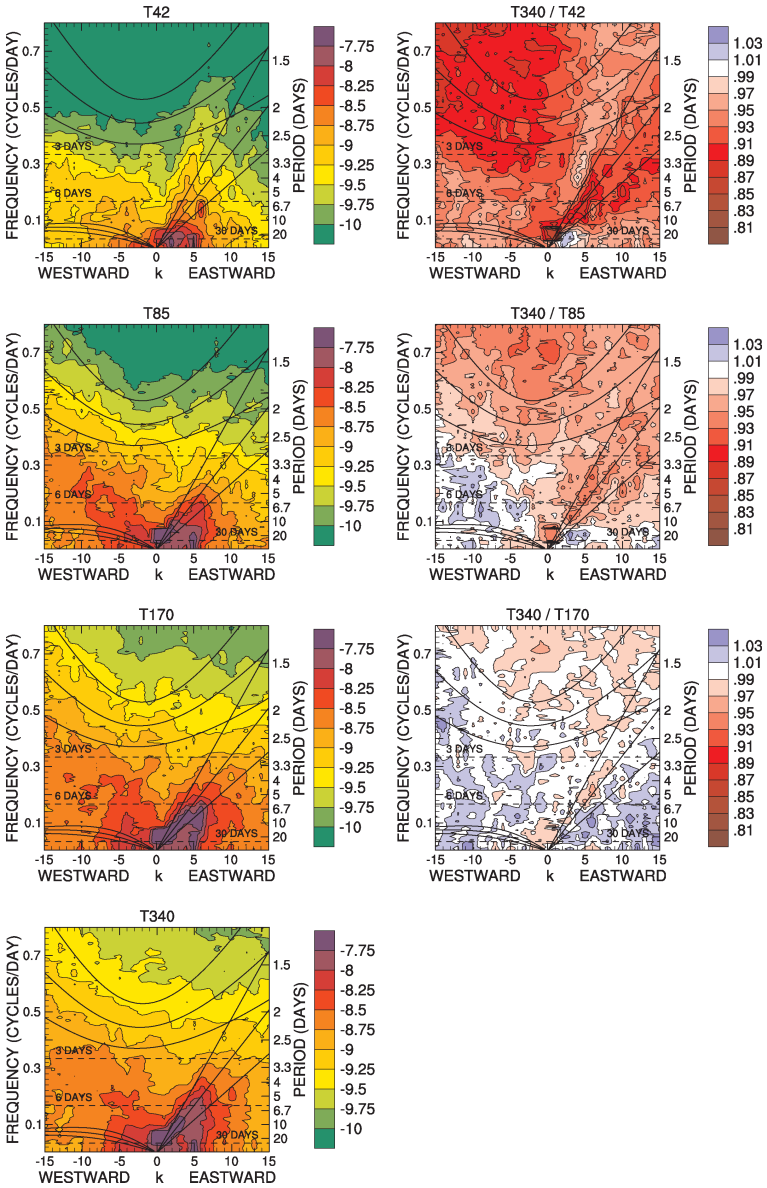

Fig. 7. Wavenumber-frequency diagrams of log of power of equatorial precipitation for (left-hand column) T42, T85, T17 and T340 with $\Delta t = 5$ min; and (right-hand column) T42, T85 and T170 normalized by T340. Values less than 1 imply the lower resolution has less power than the T340.

is the fraction of the time the precipitation is exactly 0 (there is no negative precipitation in these simulations), and the rightmost bin the fraction of time the precipitation exceeds 120 or 1200 mm d^{-1}. The distributions as a function of time step from the T42, T85 and T170 simulations are shown in the first, second and third rows, respectively, of the figure. With all resolutions there is an increase in the probability of larger precipitation with decreasing time step. Perhaps each resolution is converging to its own value since the two shortest time steps are relatively close to each other for both the T42 and the T85 simulations. A third T170 simulation with 2.5 min time step would be needed to confirm convergence of T170.

The bottom row in Fig. 8 shows the sensitivity to resolution from T42 to T340 for 5 min time step simulations. We note that plots from T42 and T85 simulations with ∇^6 diffusion (not shown) are very similar to corresponding ones in Fig. 8. There is a slight sensitivity at the highest precipitation rates but the differences are negligible compared to the differences between resolutions. Figure 8 shows that the probability of larger precipitation increases with increasing resolution with no indication of convergence. However, the figure does suggest convergence up to a certain fraction of the upper limit of precipitation at each resolution. The curves diverge from the T340 at increasing precipitation rates as resolution increases. The increasing probability with increasing resolution may be due to the inclusion of smaller scales in the higher resolution simulations. Figure 9 examines this possibility. The panels show the probabilities when the precipitation is conservatively averaged to

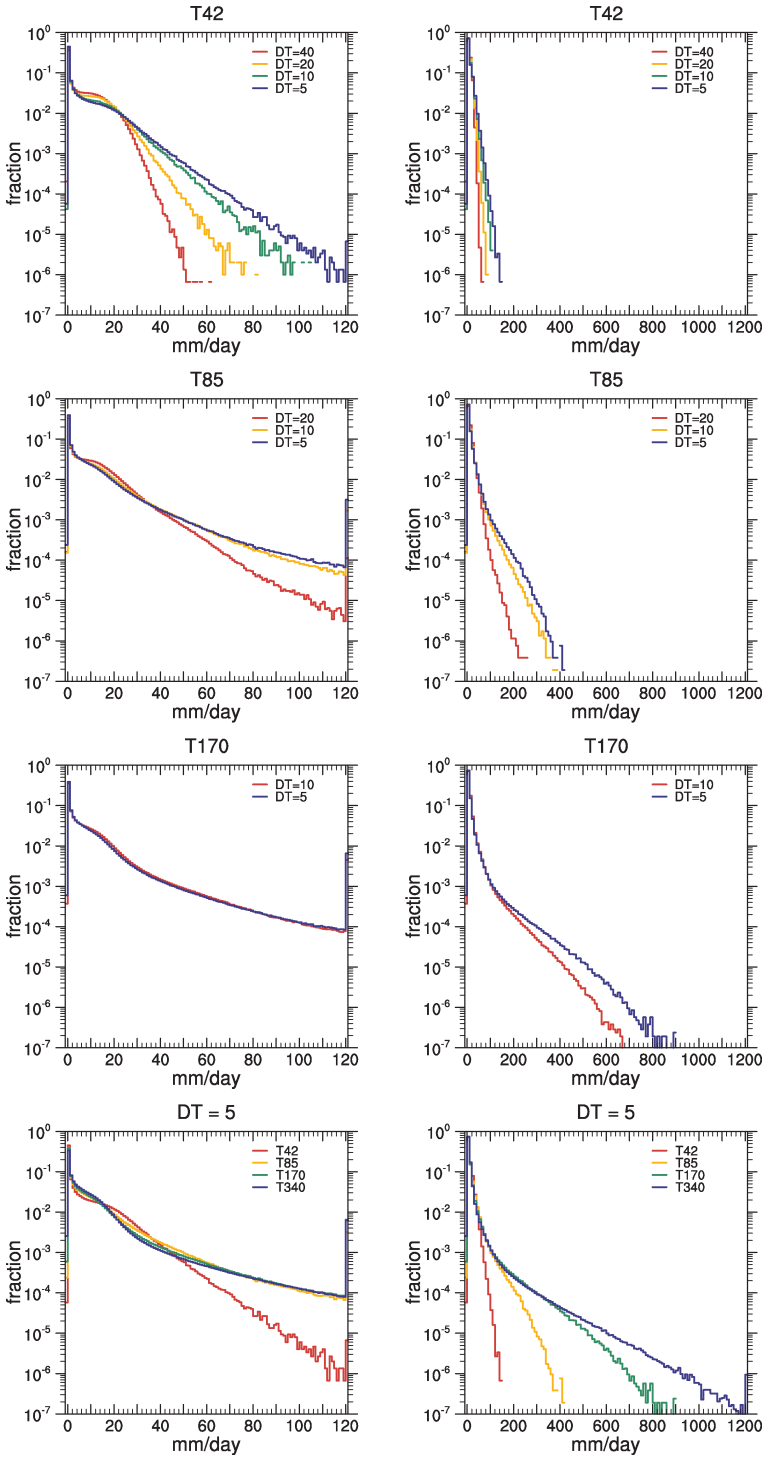

Fig. 8. Fraction of time precipitation is in (left-hand side) 1 mm d^{-1} bins ranging from 0 to 120 mm d^{-1} and (right-hand side) 10 mm d^{-1} bins ranging from 0 to 1200 mm d^{-1}. First row, T42 with $\Delta t = 40$, 20, 10 and 5 min; second row, T85 with $\Delta t = 20$, 10 and 5 min; third row, T170 with $\Delta t = 10$ and 5 min; and fourth row, T42, T85, T170 and T340 with $\Delta t = 5$ min.

larger scales before calculating the distribution. The averaging is done in grid space but we will refer to the scale by the spectral truncation normally associated with each grid. Consider first the pair in the second row. These show the probability when the precipitation is averaged to T42 scales. Here the T85, T170 and T340 simulations are all rather similar to each other, but markedly different from the T42. This implies convergence at T85 and that the model with T85 truncation is required to capture the larger T42 scales. The pair in the third row shows the probability when the precipitation is averaged to T85 scales. Now the T170 and T340 are similar to each other, but markedly different from the T85. This implies that the model with T170 resolution

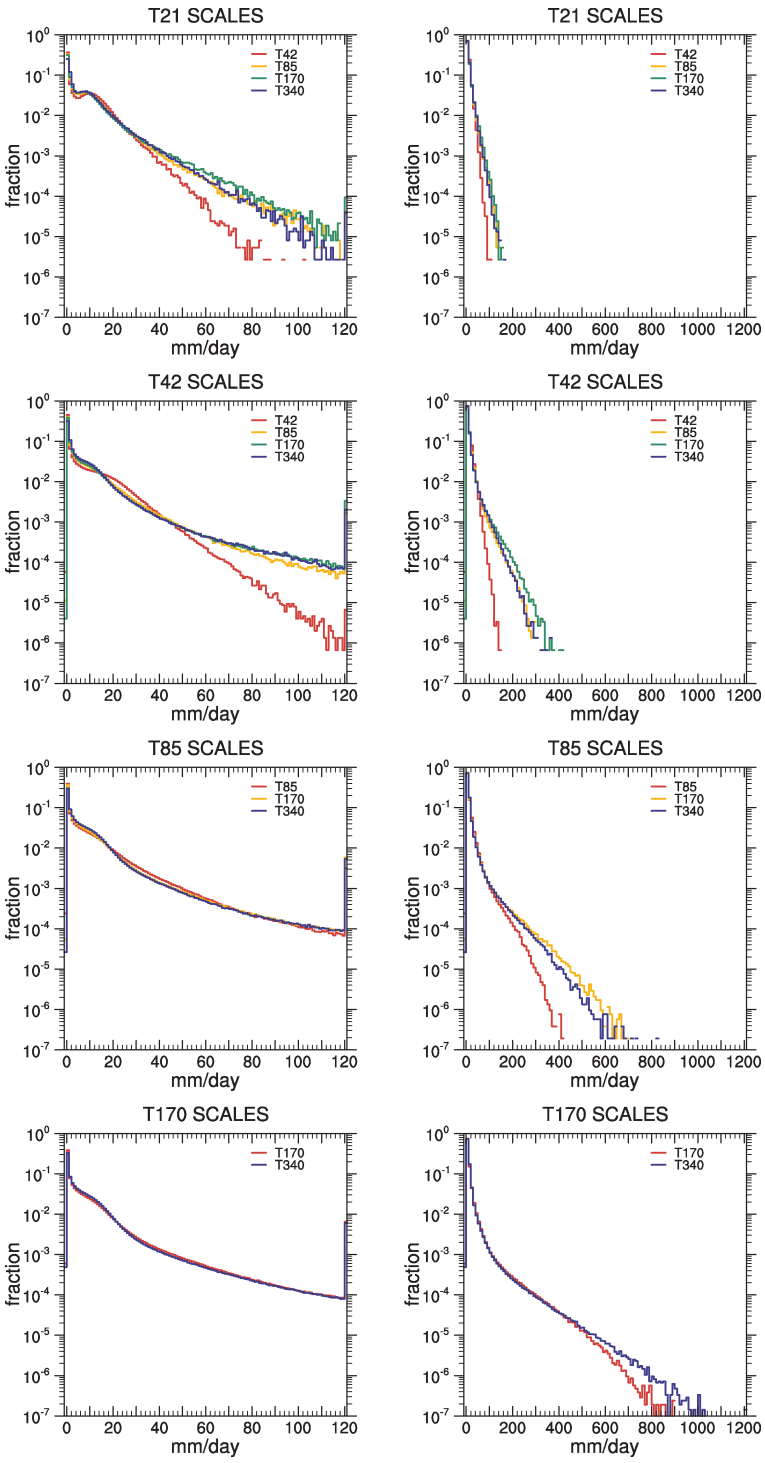

Fig. 9. Fraction of time precipitation is in (left-hand side) 1 mm d^{-1} bins ranging from 0 to 120 mm d^{-1} and (right-hand side) 10 mm d^{-1} bins ranging from 0 to 1200 mm d^{-1}, all with $\Delta t = 5$ min. First row, T42, T85, T170, T340 averaged to T21 scales before calculation; second row, T42, T85, T170, T340 averaged to T42 scales before calculation; third row, T85, T170, T340 averaged to T85 scales before calculation; and fourth row, T170, T340 averaged to T170 scales before calculation.

is required to capture the T85 scales. The pair in the bottom row shows the precipitation averaged to T170 scales. The T340 remains different from the T170, implying that, similar to the situation at lower resolutions, the T170 truncation does not capture the T170 scales. We cannot conclude that T340 does since we do not have a higher resolution simulation which might indicate convergence of the T170 scales. This analysis implies that extremes should be analysed on spatial scales larger than double the truncation limit of these models. The smallest half of the scales should not be included. The pair in the upper row, however, indicates that this conclusion holds for T85 and higher resolutions, but not for T42 and, by implication, lower. This pair shows the

precipitation averaged to T21 scales. We do not have a T21 simulation, but even the T42 simulation does not capture the T21 scales. It remains different from the T85, T170 and T340 which are all rather similar. Thus a model with T85 truncation is required to capture the T21 scales, and T42 truncation is not adequate.

9. Conclusions

We have considered the convergence of simulations with increasing horizontal resolution. The study is based on an Aqua Planet Experiment (APE) using the 'CONTROL' case defined by Neale and Hoskins (2000). The aqua-planet approach includes the full complexity of the atmospheric model including the complete parametrization suite, but simplifies the lower boundary exchange by specifying the temperature of a water covered surface. The experiments here specify the sea surface temperature to be zonally symmetric with a meridional distribution that is well resolved by a T42 spectral truncation, the lowest resolution considered. Since the aqua-planet has no land–sea contrast, no mountains and, in our case, no longitudinal variation in the SST, there is no forced asymmetric component in the solutions. The climate produced by such a scenario consists primarily of free motions. The model used is the Eulerian spectral transform based Community Atmosphere Model, CAM3 (Collins et al., 2004, 2006b)

We first mimicked a typical resolution study by comparing the time averaged, zonal averaged precipitation from the tuned T42 version of the model with that from the tuned T85 version. This 'resolution' change was further partitioned into a sequence of changes from lower to higher resolution: (1) reduction of time step from T42 to T85 value, (2) reduction in grid interval from T42 to T85 value, (3) increase in spectral truncation from T42 to T85, (4) decrease in horizontal diffusion from T42 to T85 value and (5) change in adjustable constants in the parametrizations from tuned T42 values to tuned T85 values of the standard, released model. Each member of this sequence is responsible for a rather modest change. However, they are all in the same direction and they accumulate to give a rather large change in the zonal averaged precipitation in the equatorial region.

Since in this paper we are primarily interested in the question of convergence with increasing resolution of dynamic cores coupled to a parametrization suite, in all other experiments we do not change the adjustable constants in the parametrization suite and set them to the standard T85 model values for all model resolutions. This avoids folding tuning sensitivities into the mix, but also can lead to some suboptimal aspects of the climate. One could also apply the parametrizations to coarser scales than those of the dynamics as proposed by Lander and Hoskins (1997) or consider the convergence of the system when the scale of the parametrizations is held fixed as in Williamson (1999). Such approaches are complementary to the approach considered here, which is closer to typical climate models. Such other convergence strategies should be considered as well as they might provide different insights into the convergence issue. In addition to holding the adjustable constants fixed we consider the time step and the horizontal resolution components separately. Under horizontal resolution we combine the grid, truncation and diffusion aspects since with many numerical approximations it is not obvious how to isolate these individual components.

With many explicit numerical schemes the time step and the horizontal resolution are coupled by a computational stability condition. As the resolution is increased the time step must be decreased. Models are normally run with the longest time step feasible for economical reasons. Here we compare simulations from the spectral transform CAM3 with T42, T85, T170 and T340 truncations. The time steps Δt normally applied at these resolutions are 20, 10, 5 and 2.5 min, respectively. Previous experience (Williamson and Olson, 2003) indicated that the time step of the dynamic core does not affect atmospheric simulations, but the time step over which the parametrizations are calculated does. Therefore, in this paper we refer to the centred $2\Delta t$ time steps (40, 20, 10 and 5 min) over which the parametrizations are applied, rather than the nominal time step of the dynamic core. This is intended to prevent confusion in additional studies which use two-time-level approximations rather than the centred three-time-level used here. For each spectral truncation, simulations are made with each shorter time step in this list for which that resolution is stable.

In general, the simulations show a sensitivity to the parametrization time step as well as to the horizontal resolution. For most statistics considered here these sensitivities are in the same sense, that is, shorter time step and higher resolution both lead to changes of statistics in the same direction. Thus the pure time step signal amplifies the pure horizontal resolution signal. The zonal average equatorial precipitation shows a strong sensitivity to time step. At the coarsest T42 resolution, the maximum with the shortest time step is almost double that with the longest. There is also a modulation of the shape associated with the time step. It is unsatisfactory to have such a strong sensitivity to the time step and parametrizations should be developed to be independent of time step, or failing that, they should be applied in a range of time steps where the simulations are independent of time step.

The remaining conclusions with regard to resolution alone apply to the situation where all the simulations use the same parametrization time step, 5 min, the shortest one considered. The global averages do not converge with increasing resolution for all fields. For example, there is no indication that either precipitable water or precipitation has converged by T340. The variation in the zonal average equatorial precipitation with resolution is smaller than the variation with time step. The actual peak of the equatorial maximum becomes narrower with increasing resolution indicating that some of this variation may be due to the smaller scales included in the higher resolution representations. The equatorial values do appear to converge when

conservatively averaged to a 5° grid. This implies that the larger scales in the equatorial region have converged and the variation in the global average comes from the remainder of the domain.

The convergence of the large-scale component of the zonal average of surface pressure and cloud fraction was studied. The surface pressure indicates that there is shift in the atmospheric mass from polar to equatorial regions with increasing resolution. This shift is of very large-scale and represented by the first and second symmetric associated Legendre functions. The higher modes have converged. For example the graphs of the zonal average (zonal wavenumber $m = 0$) comprised of Legendre functions (P_n^m) for $n = 12$ to the truncation limit of each model lie on top of each other for all resolutions.

The zonal average cloud fraction shows a strong resolution signal which is primarily in the global average ($n = 0$). The cloud fraction decreases with increasing resolution and the difference between adjacent resolutions appears to be increasing with increasing resolution which is opposite what one would see if the fields were converging with increasing resolution. The variation with resolution in the higher indexed associated Legendre functions is small compared to the global average although the sum over all modes does contribute to a change with resolution in the polar region. The lack of convergence of both the surface pressure and fraction is associated with smaller scales, but in different ways. The surface pressure distribution is determined by the non-linear poleward eddy momentum flux forcing the zonal mean flow. The cloud fraction is a linear average of the local cloud fraction which is dependent on the resolution.

The lack of convergence of the global average and largest meridional scales is somewhat disconcerting. In these experiments the adjustable constants in the parametrizations were held fixed at the standard T85 model values. Perhaps the parametrizations require a resolution dependency. This raises the question: Should parametrizations be tuned to yield convergent solutions of simulation aspects like global averages and large-scale structures? More usually the adjustable constants are tuned at each resolution to give the best climate by some measures. This does not necessarily lead to overall convergence. Better still might be to tune the parametrizations using model forecasts based on real case studies compared to field campaign observations and very high resolution model simulations by cloud scale resolving models (Phillips et al., 2004).

The equatorial wave propagation characteristics of the simulations were examined via Wheeler and Kiladis (1999) type wavenumber-frequency diagrams. These diagrams indicate convergence with increasing resolution of the larger scale propagating wave characteristics, however a relatively high resolution of T170 is required to capture wavenumbers less than 16, the highest wavenumber plotted.

Finally we considered the convergence of extremes by calculating probability density functions of the 6-h averaged precipitation in the equatorial region between 10°S and 10°N. With all resolutions there is an increase in the probability of larger precipitation with decreasing time step but there is some indication that each resolution is converging to its own value. With the 5 min time step there is an increase in the probability of larger precipitation with increasing resolution, but no indication of convergence with increasing resolution. The increasing probability with increasing resolution is due to the inclusion of smaller scales in the higher resolution simulations. The extremes of the larger scales however do converge. This was established by conservatively averaging the precipitation to a coarser grid before calculating the probability density functions. Thus the model with T85 truncation is required to capture the extremes of the larger T42 scales. Similarly the model with T170 truncation is required to capture the extremes of the larger T85 scales. This analysis implies that extremes should be analysed on spatial scales larger than double the truncation limit of these models. The smallest half of the scales should not be included. This conclusion holds for T85 and higher resolutions, but not for T42 and lower. The T42 model does not capture the extremes of the T21 scales. At least T85 is needed to capture the extremes of the T21 scales.

10. Acknowledgments

I would like to thank Piotr Smolarkiewicz for pointing out the editorials on numerical accuracy in the Journal of Fluids Engineering, and Jerry Olson for developing the required code and running the experiments. Richard Neale and an anonymous reviewer provided useful comments. I would especially like to thank Mike Blackburn for his very insightful comments on the manuscript. This research was partially supported by the Office of Science (BER), U.S. Department of Energy, Cooperative Agreement No. DE-FC02-97ER62402. The National Center for Atmospheric Research is sponsored by the National Science Foundation.

References

Boville, B. A. 1991. Sensitivity of simulated climate to model resolution. *J. Climate* **4**, 469–485.

Cash, B. A., Kushner, P. and Vallis, G. 2007. Comment on "On the presence of annular variability in an aquaplanet model" by Masahiro Watanabe. *Geophys. Res. Lett.* **34**, L03707, doi:10.1029/2006GL027274.

Collins, W. D., Rasch, P. J., Boville, B. A., Hack, J. J., McCaa, J. R. and co-authors. 2004. Description of the NCAR community atmosphere model (CAM3.0). *NCAR Technical Note NCAR/TN-464+STR*, xii+214 pp.

Collins, W. D., Bitz, C. M., Blackmon, M. L., Bonan, G. B., Bretherton, C. S. and co-authors. 2006a. The community climate system model version 3 (CCSM3). *J. Climate* **19**, 2122–2143.

Collins, W. D., Rasch, P. J., Boville, B. A., Hack, J. J., McCaa, J. R. and co-authors. 2006b. The formulation and atmospheric simulation of the community atmosphere model version 3 (CAM3). *J. Climate* **19**, 2144–2161.

Freitas, A. 1993. Journal of fluids engineering editorial policy statement on the control of numerical accuracy. *ASME J. Fluids Eng.* **115**, 339–340.

Giraldo, F. X. and Rosmond, T. E. 2004. A scalable spectral element Eulerian atmospheric model (SEE-AM) for NWP: dynamical core tests. *Mon. Wea. Rev.* **132**, 133–153.

Giraldo, F. X., Perot, J. B. and Fischer, P. F. 2003. A spectral element semi-Lagrangian (SESL) method for the spherical shallow water equations. *J. Comput. Phys.* **190**, 623–650.

Hack, J. J., Caron, J. M., Danabasoglu, G., Oleson, K. W., Bitz, C. M. and co-author. 2006. CCSM CAM3 climate simulation sensitivity to changes in horizontal resolution. *J. Climate* **19**, 2267–2289.

Jablonowski, C. and Williamson, D. L. 2006a. A Baroclinic wave test case for dynamical cores of general circulation models: model intercomparisons. *NCAR Technical Note NCAR/TN-469+STR* available online at http://www.library.ucar.edu/uhtbin/hyperion-image/DR000790.

Jablonowski, C. and Williamson, D. L. 2006b. A baroclinic instability test case for atmospheric model dynamical cores. *Quart. J. Roy. Meteor. Soc.* **132**, 2943–2976.

Lander, J. and Hoskins, B. J. 1997. Believable scales and parameterizations in a spectral transform model. *Mon. Wea. Rev.* **125**, 292–303.

Layton, A. T. and Spotz, W. F. 2003. A semi-Lagrangian double Fourier method for the shallow water equations on the sphere. *J. Comput. Phys.* **189**, 180–196.

Machenhauer, B. 1979. The spectral method. In: *Numerical Methods used in Atmospheric Models* Volume 2 (ed. A. Kasahara). GARP Publications Series No 17, WMO and ICSU, Geneva , 121–275.

Nair, R. D., Thomas, S. J. and Loft, R. D. 2005. A discontinuous Galerkin transport scheme on the cubed sphere. *Mon. Wea. Rev.* **133**, 814–828.

Neale, R. B. and Hoskins, B. J. 2000. A standard test for AGCMs including their physical parameterizations. I: the proposal. *Atmos. Sci. Lett.* **1**, 101–107 (http:// www.idealibrary.com/links/doi/10.1006/asle.2000.0019).

Pope, V. D. and Stratton, R. A. 2002. The processes governing horizontal resolution sensitivity in a climate model. *Clim. Dyn.* **19**, 211–236.

Phillips, T. J., Potter, G. L., Williamson, D. L., Cederwall, R. T., Boyle, J. S. and co-authors. 2004. Evaluating parameterizations in general circulation models: climate simulation meets weather prediction. *Bull. Amer. Meteor. Soc.* **85**, 1903–1915.

Roache, P. J., Ghia, K. N. and White, F. M. 1986. Editorial Policy statement on the control of numerical accuracy. *ASME J. Fluids Eng.* **108**, 2.

Roeckner, E., Brokopf, R., Esch, M., Giorgetta, M., Hagemann, S. and co-authors. 2006. Sensitivity of simulated climate to horizontal and vertical resolution in the ECHAM5 atmosphere model. *J. Climate* **19**, 3771–3791.

Stratton, R. A. 1999. A high resolution AMIP integration using the Hadley Centre model HadAM2b. *Clim. Dyn.* **15**, 9–28.

Watanabe, M. 2005. On the presence of annular variability in an aquaplanet model. *Geophys. Res. Lett.* **32**, L05701, doi:10.1029/2004GL021869.

Watanabe, M. 2007. Reply to comment by B. A. Cash et al. on "On the presence of annular variability in an aquaplanet model". *Geophys. Res. Lett.* **34**, L03708, doi:10.1029/2006GL028669.

Wheeler, M. C. and Kiladis, G. N. 1999. Convectively coupled equatorial waves: analysis of clouds and temperature in the wavenumber-frequency domain. *J. Atmos. Sci.* **56**, 374–399.

Williamson, D. L. 1999. Convergence of atmospheric simulations with increasing horizontal resolution and fixed forcing scales. *Tellus* **51A**, 663–673.

Williamson, D. L. 2008. Equivalent finite volume and spectral transform horizontal resolutions established for aqua-planet simulations. *Tellus* **60A**, doi:10.1111/j.1600-0870.2008.00340.x.

Williamson, D. L. and Olson, J. G. 2003. Dependence of aqua-planet simulations on time step. *Quart. J. Roy. Meteor. Soc.* **129**, 2049–2064.

Williamson, D. L., Drake, J. B., Hack, J. J., Jakob, R. and Swarztrauber, P. N. 1992. A standard test set for numerical approximations to the shallow water equations in spherical geometry. *J. Comput. Phys.* **102**, 211–224.